Continuous-variable Bell nonlocality with biphotons produced by spontaneous parametric down-conversion

Jonas B. Araujo,[1,*] I. G. da Paz,[2,†] Helder A. S. Costa,[2,‡] Carlos H. S. Vieira,[3,§] and Marcos Sampaio[3,‖]

[1]*Departamento de Física Matemática, Instituto de Física, Universidade de São Paulo, C.P. 66.318, São Paulo, SP 05315-970, Brazil*

[2]*Universidade Federal do Piauí, Departamento de Física, Teresina, PI 64049-550, Brazil*

[3]*CCNH, Universidade Federal do ABC, Santo André, SP 09210-580, Brazil*

(Received 4 January 2020; accepted 9 March 2020; published 1 April 2020)

We revisit a continuous-variable version of the Clauser-Horne-Shimony-Holt inequality with sign binning, first proposed by Bell [J. S. Bell, *Speakable and Unspeakable in Quantum Mechanics*, 1st ed. (Cambridge University, New York, 1987); Ann. N.Y. Acad. Sci. **480**, 263 (1986)]. To explore Bell nonlocality, we use a biphoton effective wave function resulting from a type-I spontaneous parametric down-conversion process. After reviewing the approximations involved in the production and time evolution of such biphotons, we judiciously choose a series expansion for the sinc function part of the biphoton wave function in order to integrate the Wigner function. We conclude that we can qualitatively achieve Bell nonlocality within a regime in which the twin photons are described.

DOI: 10.1103/PhysRevA.101.042103

I. POSITION-MOMENTUM CORRELATIONS AND BELL NONLOCALITY OF SPONTANEOUS PARAMETRIC DOWN-CONVERSION BIPHOTONS

Bell nonlocality indicates correlations that are incompatible with local hidden variable theories. It explains quantum correlations between spacelike separated measurement outcomes as due exclusively to past common causes. The demonstration of Bell nonlocality in continuous-variable systems is of particular interest because their high dimensionality offer the possibility of transmitting more information than with discrete variables such as spins or polarizations. In this sense, Bell nonlocality in continuous observables has traditionally used low-dimensional observables derived from the continuous observables of interest such as pseudospin observables [1] or parity observables [2]. Statistics of discrete functions such as binning functions (quadratures) of continuous observables have also been employed. For instance, in a root binning process, continuous-variable measurements are transformed into binary results which serve as input to a Bell inequality [3]. Bell himself demonstrated that the position momentum correlations of maximally entangled Einstein-Podolsky-Rosen states translated into sign binning statistics cannot violate a Bell inequality since they admit an underlying local hidden variable theory [4]). However, [5] verified continuous-variable Bell nonlocality with transverse spatial statistics of entangled photon pairs via a violation of the Clauser-Horne-Shimony-Holt (CHSH) inequality [6]. The measurements were effected at different propagation distances leading to a maximum achievable violation that is small as compared to the upper limit $2\sqrt{2}$ (for the state first considered by Bell).

Entangled photon pairs produced in spontaneous parametric down-conversion (SPDC) consist of signal and idler photons with different wavelengths, satisfying energy-momentum conservation. The names signal and idler are historical leftovers: in the early days of SPDC, most of the experiments were done with nondegenerate processes. One radiation was in the visible range (and thus easily detected, the signal), and the other was in the IR range (usually not detected, the idler) [7]. Photon pairs emitted from such sources have a high degree of correlation in time and energy as well as entanglement in frequency, polarization, and angular momentum [8]. Quantum properties of SPDC photons date back to 1970 [9], when simultaneous generation of SPDC photons was first demonstrated.

In this paper we explore a continuous-variable CHSH inequality to assess the possibility of Bell's nonlocality with sign binning position detection over time. The parties are the signal and idler photons produced by type-I SPDC. We review the derivation of the effective wave function of biphotons produced in such a process in Sec. II. For pedagogical reasons we exhibit some of the details of the derivation as some crucial approximations are not clear in the literature. We discuss the validity of the double-Gaussian approximation and present a series expansion for the sinc function that describes the transversal propagation of the biphotons. In Sec. III we discuss the effective time evolution in the Fresnel approximation, in consonance with the approximations that led to the biphoton wave function. Such physical realization of the wave function enables us to build a continuous-variable Bell inequality with sign binning, as shown in Sec. IV, by evaluating the probability that a measurement of the biphoton's position disagrees in sign just as proposed by Bell in [4].

*jbaraujo@if.usp.br
†irismarpaz@ufpi.edu.br
‡helderfisica@gmail.com
§vieira.carlos@ufabc.edu.br
‖marcos.sampaio@ufabc.edu.br

Continuous-variable CHSH inequality with sign binning

When formulating a Bell inequality to test nonlocality one should bear in mind that many current tests may rely on how a CHSH-like inequality is constructed. Some reasonable assumptions such as local causality,[1] locality, fair sampling, and the setting's independence may fail in the physical real world and it is worthwhile testing to which extent they can be relaxed [10].

The continuous-variable sign binning CHSH inequality described in [5] attributes a local hidden variable λ to explain away correlations between position measurements y_1 and y_2 of a pair of particles (say, a biphoton produced via SPDC). The joint probability density for position measurement outcomes can be generically written as

$$\rho(y_1, y_2) = \int d\lambda\, \rho(\lambda)\rho(y_1|\lambda)\rho(y_2|\lambda), \tag{1}$$

for some general distribution law for the variable λ such that $\int \rho(\lambda)d\lambda = 1$. The violation of a CHSH inequality excludes the possibility that the joint probability density is described as in Eq. (1), meaning that all information in the past light cones of such particles cannot account for the correlations between them, under the assumption of locality. Assume y a random real variable and a function $f(y) \in [-1, 1]$ and call α and α' (β and β') the measurement settings for particle 1 (2), analogous to the directions along which spins or polarizations are measured in a Einstein-Podolski-Rosen-Bohm situation. For instance, measurements at different times $t_{\alpha,\beta,\alpha',\beta'}$ may serve to conceive a CHSH-like inequality [4]. Hence the position statistics can be described by a local hidden variable model such that

$$\langle f(y_1)f(y_2)\rangle_{\alpha,\beta} = \int d\lambda\, \rho(\lambda)\langle f(y_1)\rangle_{\alpha,\lambda}\langle f(y_2)\rangle_{\beta,\lambda} \tag{2}$$

is the correlation function for all measurement outcomes y and $f(y) \in [-1, 1]$. This leads to a CHSH-like inequality as described in [5]:

$$\begin{aligned}&|\langle f(y_1)f(y_2)\rangle_{\alpha,\beta} - \langle f(y_1)f(y_2)\rangle_{\alpha,\beta'}| \\ &\quad \mp\big(\langle f(y_1)f(y_2)\rangle_{\alpha',\beta} + \langle f(y_1)f(y_2)\rangle_{\alpha',\beta'}\big) \leqslant 2,\end{aligned} \tag{3}$$

which holds in compliance with (1).

II. EFFECTIVE WAVE FUNCTION FOR A SPDC BIPHOTON

Because the nature of the approximations to obtain the final form of the biphoton wave function is important in our analysis, in this section we outline a first-principles derivation of an effective wave function for biphotons produced via SPDC as presented in [11–14]. Although this is a very well-known result, its derivation is often obscure in the literature given the many hierarchical approximations that are carried out.

[1]In the sense that measurement outcomes at one detector cannot depend on the settings or outcomes at a distant detector as well as experimenters' ability to select detector settings freely, independent of any "hidden variables" that might affect the outcomes of measurements [10].

Schematically speaking, SPDC occurs when a nonlinear and usually birefringent crystal is hit by an incoming photon at a certain (pump) frequency ω_p which in turn is converted into two new outgoing photons of lower energy ω_s (signal) and ω_i (idler). The polarization properties of the photon pair define the resulting spatial distribution and serve to characterize the SPDC phenomenon. A type-I SPDC process happens when the polarizations of the new pair of photons are parallel to each other and orthogonal to the polarization of the incoming photon. The spatial distribution of the emerging photons forms a cone that is aligned with the pump beam propagation with the apex at the crystal. If the signal and idler photons share the same polarization with each other and with the destroyed pump photon, we have a type-zero SPDC. Finally if the emergent photons have perpendicular polarization we have a type-II SPDC process and, created by the crystal forms, two (not necessarily collinear) cones that are oriented along the propagation of the pump beam and share the same apex. The process is called a parametric process, meaning that the total energy and total momentum are conserved ($\omega_p = \omega_i + \omega_s$ and $\vec{k}_p = \vec{k}_i + \vec{k}_s$). Therefore, the energies and momenta of the outgoing photons are highly correlated, and their joint quantum state is entangled. Biphoton states can be produced such that they are correlated in their spatial, temporal, spectral, or polarization properties [15]. In a typical biphoton interference experiment [16,17], a β-BBO (barium boron oxide or barium borate) nonlinear crystal of volume $\approx$200 mm^3 is pumped by a 300–400-mW argon laser emitting at $\lambda = 351.1$ nm. In [16], type-II down-converted degenerate biphotons of wavelength 702.2 nm were interfered in a double slit experiment in order to measure the de Broglie wavelength of the biphoton wave packet. The width of the slits (with its plane perpendicular to the pump laser beam direction) measured 0.1 mm, with their centers separated by 0.3 mm. Fourth-order interference patterns were obtained by coincidence counts between two detectors as a function of the two-photon detector transverse position. The detectors were placed at 690 mm after the slit plane, oriented parallel to the double slit.

The Hamiltonian of the electromagnetic field in the Coulomb gauge reads

$$\mathcal{H} = \frac{1}{2}\int d^3r\, (\vec{\mathbf{D}}\cdot\vec{\mathbf{E}} + \vec{\mathbf{B}}\cdot\vec{\mathbf{H}}), \tag{4}$$

with $\vec{\mathbf{D}} = \epsilon_0\vec{\mathbf{E}} + \vec{\mathbf{P}}$. SPDC is a $\chi^{(2)}$ process in the sense that we expand the polarization field $\vec{\mathbf{P}}$ as a power series up to the quadratic term in the electric-field strength:

$$\vec{\mathbf{P}} \approx \epsilon_0[\chi^{(1)}\vec{\mathbf{E}} + \chi^{(2)}(\vec{\mathbf{E}})^2]. \tag{5}$$

To this order, the Hamiltonian in the medium is a sum of a linear and a nonlinear term which is responsible for the conversion of the pump (p) photon into signal (subscript 1) and idler (subscript 2) photons. The nonlinear term reads

$$\begin{aligned}\mathcal{H}_{\chi^2} = \frac{\epsilon_0}{2(\sqrt{2\pi})^3}\int d^3r \sum_{\vec{\mathbf{k}}_p,\vec{\mathbf{k}}_1,\vec{\mathbf{k}}_2}\sum_{i,j,l}\tilde{\chi}^{(2)}_{ijl}(\omega_p,\omega_1,\omega_2) \\ \times E_i(\omega_p)E_j(\omega_1)E_l(\omega_2),\end{aligned} \tag{6}$$

where $\omega_{p,1,2}$ stand for $\omega_{\vec{\mathbf{k}}_p}$, $\omega_{\vec{\mathbf{k}}_1}$, $\omega_{\vec{\mathbf{k}}_2}$ and the second-order nonlinear susceptibility tensor $\tilde{\chi}^{(2)}_{ijl}$ $(i,j,l)=(x,y,z)$ depends on the photon frequencies. We perform field quantization in a box of volume V so that

$$\begin{aligned}\hat{E}(\vec{\mathbf{r}},t) &= \sum_{\vec{\mathbf{k}},s} E_0(\vec{\mathbf{k}})\,\vec{\epsilon}_{\vec{\mathbf{k}},s}\,[\hat{a}_{\vec{\mathbf{k}},s}(t)\,e^{i\vec{\mathbf{k}}\cdot\vec{\mathbf{r}}}+\text{H.c.}]\\ &\equiv \hat{E}^{+}(\vec{\mathbf{r}},t)+\hat{E}^{-}(\vec{\mathbf{r}},t),\end{aligned} \tag{7}$$

where $E_0(\vec{\mathbf{k}})=\sqrt{\hbar\omega_{\vec{\mathbf{k}}}/(2\epsilon_0 V)}$. Thus we have

$$\hat{\mathcal{H}}=\sum_{\vec{\mathbf{k}},s}\hbar\omega_{\vec{\mathbf{k}}}\hat{a}^{\dagger}_{\vec{\mathbf{k}},s}\hat{a}_{\vec{\mathbf{k}},s}+\frac{\epsilon_0}{2}\int d^3r\;\tilde{\chi}^{(2)}_{ijl}\hat{E}_i\hat{E}_j\hat{E}_l, \tag{8}$$

with $\hat{E}_{i,j,l}=\hat{E}_{i,j,l}(\vec{\mathbf{r}},t)$ and a summation over i,j,l is implicit. The last term on the right-hand side in Eq. (8) contains eight $\chi^{(2)}$ processes, including energy nonconserving ones, which can be neglected in rotating wave approximation just as in the Jaynes-Cummings model [18]. Such energy nonconserving terms oscillate with frequency ω and are proportional to $\text{sinc}(\omega T/2)$, which is negligible for large ω, T being the time to traverse the crystal. On the other hand, energy conserving processes include those with no initial output and pump photons are annihilated whereas signal-idler biphotons are created. It is usual to treat the pump beam source as a classical source that is a continuous source of pump photons. That is because the probability of generating the SPDC photon is very small (1 in 1×10^6) and thus the pump field must be very strong compared to the daughter signal and idler photon field. Hence,

$$\begin{aligned}\hat{\mathcal{H}}_{\chi^2}=\frac{\epsilon_0}{2}\int d^3r\Bigg[&\sum_{\vec{\mathbf{k}}_1,s_1,\vec{\mathbf{k}}_2,s_2}\tilde{\chi}^{(2)}_{ijl}(\vec{\mathbf{r}};\omega_p,\omega_1,\omega_2)\\ &\times E_i(\vec{\mathbf{r}},t)\,E_0(\vec{\mathbf{k_1}})\,E_0(\vec{\mathbf{k_2}})\,e^{-i(\vec{\mathbf{k}}_1+\vec{\mathbf{k}}_2)\cdot\vec{\mathbf{r}}}\\ &\times\hat{a}^{\dagger}_{\vec{\mathbf{k}}_1,s_1}(t)\,\hat{a}^{\dagger}_{\vec{\mathbf{k}}_2,s_2}(t)\,\left(\vec{\epsilon}_{\vec{\mathbf{k}}_1,s_1}\right)_j\left(\vec{\epsilon}_{\vec{\mathbf{k}}_2,s_2}\right)_l+\text{H.c.}\Bigg].\end{aligned} \tag{9}$$

Next we may assume that the pump field is narrow band around ω_p, which amounts to setting

$$E_i(\vec{\mathbf{r}},t)=e^{-i\omega_p t}E_i(\vec{\mathbf{r}}). \tag{10}$$

Taking the longitudinal direction along the $\hat{z}$ axis, we write $\vec{\mathbf{k}}_p=\vec{\mathbf{k}}_p^{\,L}+\vec{\mathbf{k}}_p^{\,T}$ and $\vec{\mathbf{k}}_{1,2}=\vec{\mathbf{k}}^{\,L}_{1,2}+\vec{\mathbf{k}}^{\,T}_{1,2}$ and we set $(\vec{\mathbf{k}}_p^{\,T};\vec{\mathbf{k}}_p^{\,L})\equiv(\vec{\mathbf{q}}_p;k_{pz}\hat{z})$ and $(\vec{\mathbf{k}}^{\,T}_{1,2};\vec{\mathbf{k}}^{\,L}_{1,2})\equiv(\vec{\mathbf{q}}_{1,2};k_{1z,2z}\hat{z})$. A further approximation consists of factoring out the longitudinal dependence of the pump field (the longitudinal component of its momentum dominates over all others),

$$E_i(\vec{\mathbf{r}},t)=\frac{1}{2\pi}\int d^2\vec{\mathbf{q}}_p\;\tilde{E}_i(\vec{\mathbf{q}}_p,t)e^{i(\vec{\mathbf{q}}_p\cdot\vec{\mathbf{r}})}e^{i(k_{pz}z-\omega_p t)}, \tag{11}$$

as well as defining the pump polarization vector such as $\tilde{E}_i(\vec{\mathbf{q}}_p,t)=\tilde{E}(\vec{\mathbf{q}}_p,t)(\vec{\epsilon}_{\vec{\mathbf{q}}_p})_i$. Taking these approximations into account enables us to write

$$\begin{aligned}\hat{\mathcal{H}}_{\chi^2}=\frac{\epsilon_0}{4\pi}\int d^3r\,d^2\vec{\mathbf{q}}_p\Bigg[&\sum_{\vec{\mathbf{k}}_1,s_1,\vec{\mathbf{k}}_2,s_2}\tilde{\chi}^{(2)}_{ijl}(\vec{\mathbf{r}};\omega_p,\omega_1,\omega_2)\\ &\times\tilde{E}(\vec{\mathbf{q}}_p,t)\,E_0(\vec{\mathbf{k}}_1)\,E_0(\vec{\mathbf{k}}_2)\,e^{-i(\Delta\vec{\mathbf{q}})\cdot\vec{\mathbf{r}}}e^{-i\Delta k_z z}e^{-i\omega_p t}\\ &\times\hat{a}^{\dagger}_{\vec{\mathbf{k}}_1,s_1}(t)\,\hat{a}^{\dagger}_{\vec{\mathbf{k}}_2,s_2}(t)\,\left(\vec{\epsilon}_{\vec{\mathbf{k}}_1,s_1}\right)_j\left(\vec{\epsilon}_{\vec{\mathbf{k}}_2,s_2}\right)_l\left(\vec{\epsilon}_{\vec{\mathbf{q}}_p}\right)_i+\text{H.c.}\Bigg],\end{aligned} \tag{12}$$

where $\Delta\vec{\mathbf{q}}\equiv\vec{\mathbf{q}}_1+\vec{\mathbf{q}}_2-\vec{\mathbf{q}}_p$ and $\Delta k_z\equiv k_{1z}+k_{2z}-k_{pz}$.

In order to perform some of the integrations in the effective Hamiltonian (12), let us specify the geometrical and experimental arrangement of such experiments. Assume a parallelepipedal isotropic crystal centered at $\vec{\mathbf{r}}=0$ so that the susceptibility tensor does not depend on $\vec{\mathbf{r}}$. As observed in [11], in order to simplify the calculations one may experimentally minimize and neglect multiple internal reflections. Using that $\int_{-L/2}^{L/2}\exp(-i\,\Delta\,x)dx=L\,\text{sinc}(L\Delta/2)$ yields

$$\begin{aligned}\hat{\mathcal{H}}_{\chi^2}=\frac{\epsilon_0}{4\pi}\int d^2\vec{\mathbf{q}}_p\Bigg[&\sum_{\vec{\mathbf{k}}_1,s_1\vec{\mathbf{k}}_2,s_2}\tilde{\chi}^{(2)}_{ijl}\tilde{E}(\vec{\mathbf{q}}_p,t)\,E_0(\vec{\mathbf{k}}_1)\,E_0(\vec{\mathbf{k}}_2)\\ &\times L_xL_yL_z\text{sinc}\left(\frac{\Delta q_xL_x}{2}\right)\text{sinc}\left(\frac{\Delta q_yL_y}{2}\right)\text{sinc}\left(\frac{\Delta k_zL_z}{2}\right)e^{-i\omega_p t}\\ &\times\hat{a}^{\dagger}_{\vec{\mathbf{k}}_1,s_1}(t)\,\hat{a}^{\dagger}_{\vec{\mathbf{k}}_2,s_2}(t)\,\left(\vec{\epsilon}_{\vec{\mathbf{k}}_1,s_1}\right)_j\left(\vec{\epsilon}_{\vec{\mathbf{k}}_2,s_2}\right)_l\left(\vec{\epsilon}_{\vec{\mathbf{q}}_p}\right)_i+\text{H.c.}\Bigg],\end{aligned} \tag{13}$$

where now $\tilde{\chi}^{(2)}_{ijl}=\tilde{\chi}^{(2)}_{ijl}(\omega_p,\omega_1,\omega_2)$. The nonlinear contribution to the total Hamiltonian $\hat{\mathcal{H}}=\sum_{\vec{\mathbf{k}},s}\hbar\omega_{\vec{\mathbf{k}}}\hat{a}^{\dagger}_{\vec{\mathbf{k}},s}\hat{a}_{\vec{\mathbf{k}},s}+\hat{\mathcal{H}}_{\chi^2}$ is very small with respect to the linear part. In order to calculate the biphoton state, we proceed to treat the problem in the interaction picture using first-order time-dependent perturbation theory which is accurate in most applications. The energy of the pump field is a factor of 10^8 larger (for typical experimental parameters) than the energy of the signal and idler fields. For such small corrections higher-order corrections in perturbation theory are small and may be ignored.

Moreover, considering fields with a definite polarization we may drop the $s_{1,2}$ indices (and the related sums) from (13). If the nonlinear susceptibility is a slowly varying function of the frequencies we can consider it as a constant. In a natural regime in which the crystal itself is much larger than the optical wavelengths in the experiment, it is reasonable to substitute $\sum_{\vec{\mathbf{k}}}$ with $V\int d^3\vec{\mathbf{k}}/(2\pi)^3$. Hence, in the interaction picture, where operators evolve in time with the linear piece of the Hamiltonian, e.g., $\hat{a}^{\dagger}(t)=\hat{a}^{\dagger}(0)e^{i\omega t}$, we write, for the initial vacuum state $|0_1,0_2\rangle$ [11],

$$\begin{aligned}\hat{\mathcal{H}}_{\chi^2}\approx\chi_{\text{eff}}\iint d^3\vec{\mathbf{k}}_1d^3\vec{\mathbf{k}}_2\,\sqrt{\omega_{\vec{\mathbf{k}}_1}\,\omega_{\vec{\mathbf{k}}_2}}\int d^2\vec{\mathbf{q}}_p\,\tilde{E}(\vec{\mathbf{q}}_p,t)\\ \times\text{sinc}\left(\frac{\Delta q_xL_x}{2}\right)\text{sinc}\left(\frac{\Delta q_yL_y}{2}\right)\text{sinc}\left(\frac{\Delta k_zL_z}{2}\right)\\ \times e^{i\Delta\omega t}\hat{a}^{\dagger}_{\vec{\mathbf{k}}_1}\,\hat{a}^{\dagger}_{\vec{\mathbf{k}}_2},\end{aligned}$$

in which we redefined

$$\chi_{\rm eff} = \frac{\hbar}{8\pi}\frac{L_x L_y L_z V}{(2\pi)^6}\tilde{\chi}^{(2)}_{ijl}(\vec{\epsilon}_p)_i(\vec{\epsilon}_1)_j(\vec{\epsilon}_2)_l,$$

$\Delta\omega = \omega_1 + \omega_2 - \omega_p$.

The state of the down-converted photon pair can be formally written as

$$|\Psi(t)\rangle_{\rm SPDC} \approx \left(1 - \frac{i}{\hbar}\int_0^\tau dt'\,\hat{\mathcal{H}}_{\chi^2}(t')\right)|0_1, 0_2\rangle, \tag{14}$$

where the integration runs over the time it takes for light at the pump wavelength to travel through the crystal, and it is further assumed that the pump amplitude $\tilde{E}(\vec{\mathbf{q}}_p, t)$ does not vary significantly over τ. We are left with

$$\int_0^\tau dt'\, e^{i\Delta\omega t'} = \tau e^{i\frac{\Delta\omega\tau}{2}}\,\mathrm{sinc}\left(\frac{\Delta\omega\tau}{2}\right). \tag{15}$$

in which the limit where $\Delta\omega = 0$ (energy conservation) is clearly τ. We may therefore write

$$|\Psi\rangle_{\rm SPDC} \approx C_0|0_1, 0_2\rangle + C_1\chi_{\rm eff}\iint d^3\vec{\mathbf{k}}_1 d^3\vec{\mathbf{k}}_2\,\sqrt{\omega_{\vec{\mathbf{k}}_1}\,\omega_{\vec{\mathbf{k}}_2}} \times \Phi(\vec{\mathbf{k}}_1, \vec{\mathbf{k}}_2)\hat{a}^\dagger_{\vec{\mathbf{k}}_1}\,\hat{a}^\dagger_{\vec{\mathbf{k}}_2}|0_1, 0_2\rangle, \tag{16}$$

where the biphoton wave function $\Phi(\vec{\mathbf{k}}_1, \vec{\mathbf{k}}_2)$ is, up to a normalization factor,

$$\Phi(\vec{\mathbf{k}}_1, \vec{\mathbf{k}}_2) = \left[\int d^2\vec{\mathbf{q}}_p\,\tilde{E}(\vec{\mathbf{q}}_p)\,\mathrm{sinc}\left(\frac{\Delta q_x L_x}{2}\right)\mathrm{sinc}\left(\frac{\Delta q_y L_y}{2}\right)\right] \times \mathrm{sinc}\left(\frac{\Delta k_z L_z}{2}\right), \tag{17}$$

which is quite obvious on general grounds, but the series of judicious approximations which have been performed were crucial to understand the nature of the wave-function profile.

Crystal dimensions are significantly larger than the typical photon wavelengths that cross such crystals (by a factor of 10^3–10^4 for visible wavelengths and a crystal of a few millimeters thick). Hence the sinc function factors depending on transverse coordinates act like delta functions (the only significant contributions coming from, e.g., $q_x = 0$, or when the sum of the transverse signal and idler momenta is about the same as transverse pump momentum $\vec{\mathbf{q}}_p = \vec{\mathbf{q}}_1 + \vec{\mathbf{q}}_2$). Therefore,

$$\Phi(\vec{\mathbf{k}}_1, \vec{\mathbf{k}}_2) = \mathcal{N}\delta(\omega_1 + \omega_2 - \omega_p)\delta^2(\vec{\mathbf{q}}_1 + \vec{\mathbf{q}}_2 - \vec{\mathbf{q}}_p) \times \mathrm{sinc}\left(\frac{\Delta k_z L_z}{2}\right)\tilde{E}(\vec{\mathbf{q}}_1 + \vec{\mathbf{q}}_2), \tag{18}$$

where $\mathcal{N}$ is a normalization constant.

A. Type-I SPDC $e \to oo$ twin-photon generation

We proceed to express k_z in terms of the transverse components $\vec{\mathbf{q}}$. To fulfill the matching conditions (energy momentum conservation) in SPDC, we need to have differences in refractive indices for idler, signal, and pump photons. With the help of birefringence crystals, where photons with different polarizations have different refractive indices, this task can be accomplished.

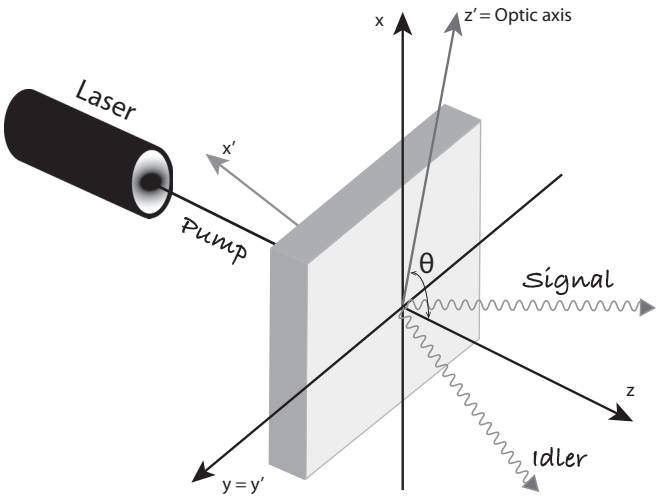

FIG. 1. Birefringence crystal. Ordinary rays have polarization in a direction perpendicular to the plane $z - z'$ defined by the propagation direction z and the optic axis z'.

In anisotropic materials the speed of light depends on the propagation direction. Such a dependence can be very complicated in general, except for uniaxial crystals. In the study of correlation properties of two-photon states, the photon pairs are generated by spontaneous parametric down-conversion in uniaxial crystals. In this case, the crystal has one axis (optical axis or extraordinary axis) along which a ray of transmitted light suffers no birefringence. Light propagates along that axis with a speed independent of its polarization. If the light beam is not parallel to the optic axis, the beam is split into two rays (the ordinary and extraordinary) when passing through the crystal. These rays will be mutually orthogonally polarized. Ordinary rays have polarization in a direction perpendicular to the plane $z - z'$ defined by the propagation direction z and the optic axis z' (Fig. 1). Such light experiences the ordinary refractive index n_o. Extraordinary rays have polarization on the plane $z - z'$ and experience a refractive index $n_e(\theta)$ that depends on the angle θ between the optical axes and z according to the relation

$$\frac{1}{n_e(\theta)^2} = \frac{\cos^2\theta}{n_o^2} + \frac{\sin^2\theta}{n_e^2}. \tag{19}$$

Notice that for $n_e(\theta = 90^\circ) = n_e$ its principal value and $n_e(\theta = 0) = n_o$. In type-I SPDC (Fig.2) the pump photon has an orthogonal polarization (either ordinary or extraordinary) with respect to idler and signal photons which are equally polarized. Due to the fact that the two photons have the same polarization they will have the same refractive index

TABLE I. SPDC type I: matching conditions.

SPDC	Positive uniaxial ($n_e > n_o$)	Negative uniaxial ($n_e < n_o$)
Type I	$n_p^o\omega_p = n_1^e\omega_1 + n_2^e\omega_2$	$n_p^e\omega_p = n_1^o\omega_1 + n_2^o\omega_2$
Type II	$n_p^o\omega_p = n_1^e\omega_1 + n_2^e\omega_2$	$n_p^e\omega_p = n_1^o\omega_1 + n_2^o\omega_2$

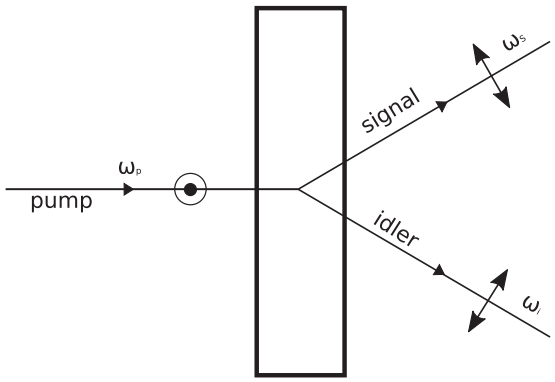

FIG. 2. Type-I SPDC process. The signal and idler photons are mutually incoherent, and thus they exhibit no second-order interference when brought together at detectors D_1 and D_2. However fourth-order interference occurs, by the coincidence counting rate between $D1$ and $D2$.

and thus lie on the same cone.[2] The pair exits the crystal either noncollinearly (propagating to different directions) or collinearly (aligned with the pump).

Uniaxial crystals are characterized by a refractive index of an ordinary ray n_o, and a refractive index of an extraordinary ray n_e. $\beta-$BBO is a negative uniaxial crystal ($n_e < n_o$). For a list of matching conditions, please see Table I

Consider the case of a type-I SPDC from a negative uniaxial crystal with an e-ray pump going to two rays ($e \to oo$) just as depicted in Fig. 1. Let us define the longitudinal phase mismatch as[3]

$$\Delta k_z \equiv k_{1z} + k_{2z} - k_{pz} = \sqrt{|\vec{\mathbf{k}}_1|^2 - |\vec{\mathbf{q}}_1|^2} + \sqrt{|\vec{\mathbf{k}}_2|^2 - |\vec{\mathbf{q}}_2|^2} - \sqrt{|\vec{\mathbf{k}}_p|^2 - |\vec{\mathbf{q}}_p|^2}. \tag{20}$$

In the Fresnel (paraxial) approximation where the longitudinal and transversal components of the momenta are such that $|\vec{\mathbf{q}}|^2 \ll |\vec{\mathbf{k}}|^2$, Eq. (20) reads, to first order in $|\vec{\mathbf{q}}|^2/|\vec{\mathbf{k}}|$,

$$\Delta k_z \approx |\vec{\mathbf{k}}_1|^2 + |\vec{\mathbf{k}}_2|^2 - |\vec{\mathbf{k}}_p|^2 + \frac{|\vec{\mathbf{q}}_p|^2}{2|\vec{\mathbf{k}}_p|} - \frac{|\vec{\mathbf{q}}_1|^2}{2|\vec{\mathbf{k}}_1|} - \frac{|\vec{\mathbf{q}}_2|^2}{2|\vec{\mathbf{k}}_2|}. \tag{21}$$

The anisotropic crystals used for SPDC are such that the longitudinal components of the wave vector will get modified by a different amount as they will realize a different refractive index inside the anisotropic medium. Phase matching is achieved by adjusting the angle θ to obtain the value $n_e(\theta)$ for which the condition $\Delta k_z = 0$ is satisfied. For this purpose, consider again the geometrical configuration represented by the coordinate systems in Fig. 1. The primed system is obtained by a rotation of θ around the y axis such that z' is parallel to the optical axis, $\vec{\mathbf{r}}' = R_y(\theta)\vec{\mathbf{r}}$. For uniaxial crystals, the dielectric tensor ε in the primed system $\vec{\mathbf{D}}' = \varepsilon\vec{\mathbf{E}}'$ is diagonal, namely, $\varepsilon = \mathrm{diag}(n_o^2, n_o^2, n_e^2)$, with $n_o^2 \equiv \varepsilon_{x'}/\varepsilon_0 = \varepsilon_{y'}/\varepsilon_0$ and $n_e^2 \equiv \varepsilon_{z'}/\varepsilon_0$. It is easy to see that in the primed system we have

$$\frac{q_{x'}^2 + q_{y'}^2 + k_{z'}^2}{n_o^2} = \frac{\omega^2}{c^2}, \tag{22}$$

$$(n_o q_{x'})^2 + (n_o q_{y'})^2 + (n_e k_{z'})^2 = \frac{\omega^2}{c^2}(n_o n_e)^2 \tag{23}$$

for the ordinary and extraordinary rays, respectively. Transforming back to the unprimed system and isolating k_z, we obtain, within the Fresnel approximation, that (22) yields

$$k_z \approx \frac{n_o\omega}{c} - \frac{c}{2n_o\omega}\left(q_x^2 + q_y^2\right), \tag{24}$$

whereas (23) becomes

$$k_z \approx \alpha q_x + \frac{n_e(\theta)\omega}{c} - \frac{c}{2n_e(\theta)\omega}\left(\beta^2 q_x^2 + \gamma^2 q_y^2\right), \tag{25}$$

where

$$\alpha = \frac{\sin 2\theta}{2} n_e^2(\theta)\left(\frac{1}{n_e^2} - \frac{1}{n_o^2}\right),\ \beta = \frac{n_e^2(\theta)}{n_o n_e},\ \gamma = \frac{n_e(\theta)}{n_e}, \tag{26}$$

with $n_e(\theta)$ given by (19). The parameter α is responsible for the walk-off, namely, the different refractive indices for signal and idler photons cause a separation of the idler and the signal beam (transversal walk-off). The terms β and γ cause a slight astigmatism in beams propagating through the uniaxial medium. Their effects are marginals and they can be approximated by 1 (see [12]). Thus, the argument of the sinc function in (18) reads

$$\frac{L_z\Delta k_z}{2} = l_t(q_{ix} + q_{sx}) + \frac{L_z}{2}(k_{oi} + k_{os} - k_{ep}) - \frac{L_z}{4}\left(\frac{|\vec{\mathbf{q}}_i|^2}{k_{oi}} + \frac{|\vec{\mathbf{q}}_s|^2}{k_{os}} - \frac{|\vec{\mathbf{q}}_i + \vec{\mathbf{q}}_s|^2}{k_{ep}}\right), \tag{27}$$

where $l_t \equiv \alpha_p L_z/2$ is the transverse walk-off length, $k_{oi} \equiv n_{oi}\omega_i/c$, $k_{os} \equiv n_{os}\omega_s/c$, and $k_{ep} \equiv n_e(\theta)\omega_p/c$. In the $e \to oo$ degenerate case, where $\omega_i = \omega_s = \omega_p/2$ and $k_{oi} = k_{os}$, we have

$$\frac{L_z\Delta k_z}{2} = l_t(q_{ix} + q_{sx}) + \frac{L_z k_{ep}}{2}\frac{(1-\delta)}{(1+\delta)} - \frac{L_z\delta}{4k_{ep}}|\vec{\mathbf{q}}_i - \vec{\mathbf{q}}_s|^2 + \frac{L_z(1-\delta)}{2k_{ep}}\vec{\mathbf{q}}_i \cdot \vec{\mathbf{q}}_s, \tag{28}$$

with

$$\delta \equiv 2\frac{n_e(\theta)}{n_o} - 1 \approx 1, \tag{29}$$

consistently with $\beta \approx \gamma \approx 1$ and $\alpha \approx 0$.

It is usual to assume that the transverse pump momentum profile is Gaussian:

$$\tilde{E}(\vec{\mathbf{q}}_i + \vec{\mathbf{q}}_s) = \tilde{\mathcal{N}} e^{-|\vec{\mathbf{q}}_i + \vec{\mathbf{q}}_s|^2/\sigma_\perp^2}. \tag{30}$$

[2]Light travels with a higher phase velocity through an axis that has the smallest refractive index and this axis is called the fast axis. Similarly, an axis which has the highest refractive index is called a slow axis since the phase velocity of light is the lowest along this axis. The optic axis can be the fast or the slow axis for the crystal depending on the material.

[3]In principle, $\Delta k_z \equiv \frac{n_1\omega_1}{c} + \frac{n_2\omega_2}{c} - \frac{n_3\omega_p}{c} = 0$ cannot be satisfied for most materials as, for "normal" dispersions, $n_1(\omega_1) \leqslant n_2(\omega_2) < n_3(\omega_p)$ for $\omega_1 \leqslant \omega_2 < \omega_p$.

Finally, we can write (18) as

$$\Phi(\vec{\mathbf{q}}_i, \vec{\mathbf{q}}_s) = \mathcal{N}_s \ \mathrm{sinc}(b^2|\vec{\mathbf{q}}_i - \vec{\mathbf{q}}_s|^2) e^{-|\vec{\mathbf{q}}_i+\vec{\mathbf{q}}_s|^2/\sigma_\perp^2}, \tag{31}$$

in which $b^2 \equiv \frac{L_z}{4k_{ep}}$, $\mathcal{N}_s$ is the normalization, and we have left out the delta functions for shortness. The minus sign in the sinc function is immaterial as it is an even function. The wave function in Eq. (31) is also obtained in the nearly collinear approximation [11,12], meaning that the approximations we have performed reflect such a hypothesis. The Gaussian with the argument $\vec{\mathbf{q}}_i + \vec{\mathbf{q}}_s$ is nothing but a statement of the uncertainty in transverse momentum conservation, whereas $\vec{\mathbf{q}}_i - \vec{\mathbf{q}}_s$ in the sinc function expresses energy and (longitudinal) momentum conservation. Moreover, the momentum space amplitude $\Phi(\vec{\mathbf{q}}_i, \vec{\mathbf{q}}_s)$ is not separable into factors depending only on $\vec{\mathbf{q}}_i$ and $\vec{\mathbf{q}}_s$ and therefore it is entangled (not factorable).

B. Double-Gaussian approximation

In [19] it is shown that the degree of entanglement is governed by the product $\sigma_\perp b$. High entanglement is achieved when either $\sigma_\perp b \gg 1$ or $\sigma_\perp b \ll 1$, the minimum occurring for $\sigma_\perp b \approx 1$. Moreover the sinc representation of the biphoton wave function is more entangled than its Gaussian approximation for the same values of $\sigma_\perp b$ [19]. In order to study the transversal correlations of the biphotons we need to Fourier transform the wave function into coordinate space. Following [11,12,16,19–22] we can approximate the sinc function by a Gaussian:

$$\Phi(\vec{\mathbf{q}}_i, \vec{\mathbf{q}}_s) = \mathcal{N}_G \ e^{-b^2|\vec{\mathbf{q}}_i-\vec{\mathbf{q}}_s|^2} e^{-|\vec{\mathbf{q}}_i+\vec{\mathbf{q}}_s|^2/\sigma_\perp^2}. \tag{32}$$

As discussed in [11], this biphoton wave function is approximately separable (subject to the paraxial approximation) into a product of functions, one dependent on only x coordinates and the other dependent on only y coordinates).[4] Let us take the y component and write q_{iy}, q_{sy} simply as q_i, q_s. Thus,

$$\Phi_S(q_i, q_s) = \widetilde{\mathcal{N}}_S \ \mathrm{sinc}[b^2(q_i - q_s)^2] e^{-(q_i+q_s)^2/\sigma_\perp^2}, \tag{33}$$

and

$$\Phi_G(q_i, q_s) = \widetilde{\mathcal{N}}_G e^{-b^2(q_i-q_s)^2} e^{-(q_i+q_s)^2/\sigma_\perp^2}. \tag{34}$$

The Fourier transforms of Eqs. (33) and (34) read, respectively,

$$\begin{aligned}\Psi_S(y_-, y_+) = \mathcal{N}_s \Bigg\{ & 2\sqrt{\pi} y_- \left[\mathcal{S}\left(\frac{y_-}{\sqrt{2\pi}\sigma_-}\right) - \mathcal{C}\left(\frac{y_-}{\sqrt{2\pi}\sigma_-}\right)\right] \\ & + 2\sqrt{2}\sigma_- \left[\cos\left(\frac{y_-^2}{4\sigma_-^2}\right) + \sin\left(\frac{y_-^2}{4\sigma_-^2}\right)\right]\Bigg\} e^{-\frac{y_+^2}{4\sigma_+^2}} \\ & \equiv \Psi_S^-(y_-)\Psi_S^+(y_+), \end{aligned} \tag{35}$$

[4]That is because for small values of x and y $\mathrm{sinc}(x+y) \sim \mathrm{sinc}(x)\mathrm{sinc}(y)$. For typical experimental parameters, the argument of the sinc function is of the order 10^{-3}, even for transverse momenta as large as the pump momentum. Taking the paraxial approximation, the transverse momenta are much smaller than the pump momentum, and so the arguments of the sinc functions are very small [11].

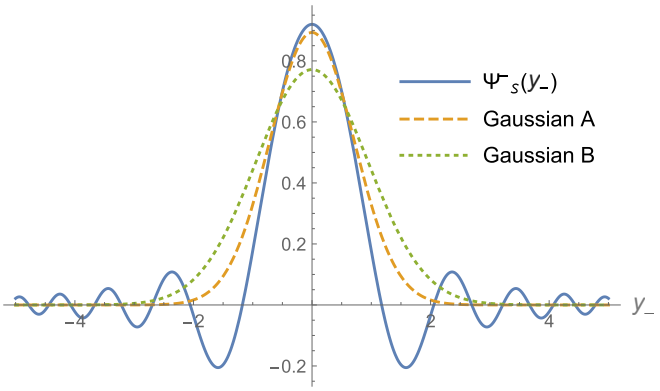

FIG. 3. Normalized $\Psi_S^-(y_-)$ and Gaussian approximation $\Psi_G^-(y_-)$ represented by Gaussian A, both for $\sigma_- = 1/(2\sqrt{2})$. Gaussian B is the normalized Gaussian of width σ_-^B such that it yields the same value for the second moment as if one had used $\Psi_S^-(y_-)$.

where $\mathcal{S}(x)$ and $\mathcal{C}(x)$ are the sine and cosine Fresnel integrals and

$$\begin{aligned}\Psi_G(y_-, y_+) &= \frac{1}{\sqrt{2\pi\sigma_-\sigma_+}} e^{-\frac{y_-^2}{4\sigma_-^2}} e^{-\frac{y_+^2}{4\sigma_+^2}} \\ &\equiv \Psi_G^-(y_-)\Psi_G^+(y_+), \end{aligned} \tag{36}$$

where $\sigma_- \equiv b/\sqrt{2}$, $\sigma_+ \equiv \sqrt{2}\sigma_\perp$, and

$$y_\pm \equiv \frac{(y_i \pm y_s)}{\sqrt{2}}.$$

Also we have normalized Ψ_G so that $\iint dy_- \, dy_+ |\Psi_G|^2 = 1$.

The transverse pump profile is assumed to be a Gaussian of width $\propto \sigma_\perp$. The sinc-based function and its Fourier transform $\Psi_S^-(y_-)$ may be approximated by a Gaussian by assuming the sinc argument to be the same as the one in the exponential of the Gaussian $\Psi_G^-(y_-)$ as displayed in (33) and (34) [19]. However, a more accurate description would be to choose a Gaussian of a certain width such that it reproduces numerically the same value for the first and second moments as calculated from $\Psi_S - (y_-)$. Taking, for instance, $\sigma_- = 1/(2\sqrt{2})$ yields $\langle \Psi_s^- | y_-^2 | \Psi_s^- \rangle = 0.449$, which was calculated using numerical integration with the MATHEMATICA local adaptive method. The width σ_-^B of the corresponding Gaussian that yields the same value is just $\sqrt{0.449}$ (see Fig. 3).

A double-Gaussian wave function is very amenable to calculations and makes both transverse position and transverse momentum statistics easy to calculate. Moreover, as we shall see, the double-Gaussian wave function is easy to propagate in the paraxial regime (the same regime we used in the approximations of our biphoton state to start with). Moreover it fits well experimental data [23]. On the other hand, the sinc function is an orthogonal wave function, which is in $\mathcal{L}^2(\mathbb{R})$ and is of interest in the study of continuous-variable quantum algorithms [24].

C. Wigner function

The Wigner function can be defined using (33) as

$$W(y_i, y_s, q_i, q_s) = \frac{1}{(2\pi)^2}\int dp_i \int dp_s\, e^{-ip_i y_i} e^{-ip_s y_s} \times \Phi_S^*\left(q_i + \frac{p_i}{2}; q_s + \frac{p_s}{2}\right) \times \Phi_S\left(q_i - \frac{p_i}{2}; q_s - \frac{p_s}{2}\right). \quad (37)$$

If we redefine $q_\pm = (q_i \pm q_s)/\sqrt{2}$ and $p_\pm = (p_i \pm p_s)/\sqrt{2}$, then

$$W(y_i, y_s, q_i, q_s) = W(y_+, y_-, q_+, q_-) \equiv W_S(y_-, q_-) W_G(y_+, q_+), \quad (38)$$

where

$$W_S(y_-, q_-) = \frac{1}{2\pi}\int dp_-\, e^{-ip_- y_-}\, \mathrm{sinc}\left[4\sigma_-^2\left(q_- + \frac{p_-}{2}\right)^2\right] \times \mathrm{sinc}\left[4\sigma_-^2\left(q_- - \frac{p_-}{2}\right)^2\right] \quad (39)$$

and

$$W_G(y_+, q_+) = \frac{1}{2\pi}\int dp_+\, e^{-ip_+ y_+}\, e^{-\frac{4}{\sigma_+^2}(q_+ + \frac{p_+}{2})^2} \times e^{-\frac{4}{\sigma_+^2}(q_+ - \frac{p_+}{2})^2}. \quad (40)$$

Following [4] we are interested in evaluating the integral $W_S(y_-, q_-)$ in Eq. (39). We can set $\sigma_-^2 = 1/4$ for convenience. Changing to a new variable $\rho = p_-/2$ and using that

$$\mathrm{sinc}\,(t) = \prod_{m=1}^{\infty} \cos\left(\frac{t}{2^m}\right) \quad (41)$$

yields

$$W_S(y_-, q_-) = \frac{2}{2\pi}\int d\rho\, e^{-2i\rho y_-} \prod_{m=1}^{M} \cos\left[\frac{(q_- - \rho)^2}{2^m}\right] \times \prod_{n=1}^{M} \cos\left[\frac{(q_- + \rho)^2}{2^n}\right]. \quad (42)$$

In the equation above it will be useful to replace the product with a summation sign using the cosine product-to-sum identity [25]

$$\prod_{m=1}^{M} \cos\left(\frac{t}{2^m}\right) = \frac{1}{2^{M-1}}\sum_{m=1}^{2^{M-1}} \cos\left(\frac{2m-1}{2^M}t\right) = \frac{2^{1-M}\cos\left(\frac{t}{2}\right)\sin\left(\frac{t}{2}\right)}{\sin(2^{-M}t)}. \quad (43)$$

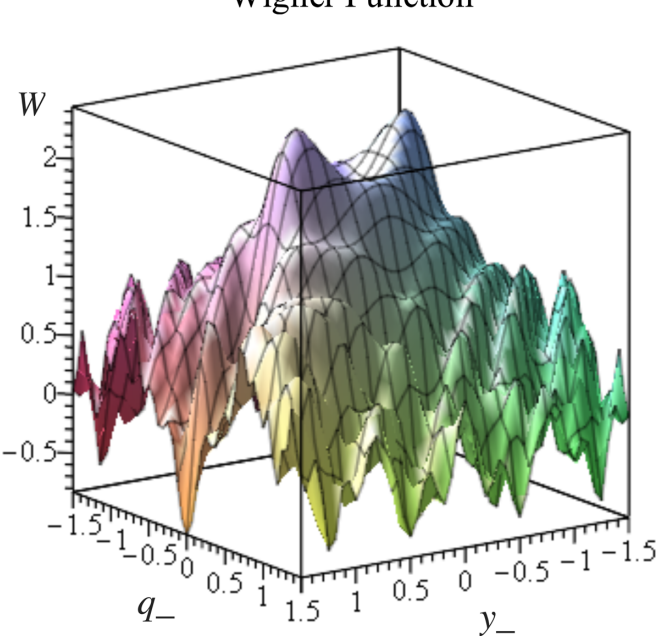

FIG. 4. Wigner function $W_S(y_-, q_-)$ for $\sigma_-^2 = 1/4$. $M = 4$ in the series in Eq. (43) already provides a very good approximation. Notice that $W_S(y_-, q_-)$ has negative values as opposite to its Gaussian approximation $W_G(y_-, q_-)$ which is always positive.

This enables us to write

$$W_S(y_-, q_-) = \frac{\mathcal{N}_S}{2^{(2M-2)}\pi}\sum_{m=1}^{2^{M-1}}\sum_{n=1}^{2^{M-1}}\int d\rho\, e^{-2i\rho y_-} \times \cos\left[\frac{2m-1}{2^M}(q_- - \rho)^2\right] \times \cos\left[\frac{2n-1}{2^M}(q_- + \rho)^2\right], \quad (44)$$

which we evaluate in the Appendix, $\mathcal{N}_S$ being a suitable normalization so that $\iint dy_- dq_-\, W_S(y_-, q_-) = 1$. On the other hand,

$$W_G(y_+, q_+) = \frac{1}{\pi} e^{-\frac{\sigma_+^2 y_+^2}{8} - \frac{8q_+^2}{\sigma_+^2}}. \quad (45)$$

In Fig. 4 we show the plot of the Wigner function $W_S(y_-, q_-)$ for $\sigma_-^2 = 1/4$. We consider $M = 6$ in the series in Eq. (43) which already provides a very good approximation. As we can observe $W_S(y_-, q_-)$ has negative values as opposite to its Gaussian approximation $W_G(y_-, q_-)$ which is always positive. This negativity is important to observe entanglement.

III. FREE PROPAGATOR FOR THE BIPHOTON WAVE FUNCTION IN THE FRESNEL APPROXIMATION

Whichever effective model one uses to describe a photon, it is important to take into account the process which generates it [26–28]. In [29] was presented a wave-function description of a photon in a Young double slit experiment in which the photon source is a single excited atom (see also [30]). Moreover, in [31] a second quantized version of the

Bialynicki-Birula-Sipe photon wave-function [32] formalism was extended to include the interaction between photons and continuous (nonabsorptive) media. As an application, the quantum state of the twin photons generated by SPDC was derived. That being said, an effective wave-function treatment of photon states is possible and tools from Schrödinger wave mechanics may provide insights on various aspects of quantum light.

In constructing the down-converted biphoton wave function we have used the Fresnel approximation. Consistently, under the conditions of validity of the Fresnel approximation, the diffraction and interference of a wave traveling in the z direction can be described in terms of its spreading in time of the wave-packet transversal (x, y) section [33]. In the case of de Broglie waves for massive particles, the wave-packet spreading is due to the nature of the dispersion relation $\omega_k = \hbar k^2/(2m)$ and the free evolution is simply given by the Fourier transform

$$\psi(\vec{r}, t) = \int d^3k \; e^{(i\vec{k}.\vec{r} - i\omega_k t)} \; \tilde{\psi}(\vec{k}, 0), \tag{46}$$

where $\tilde{\psi}(\vec{k}, 0)$ is the Fourier transform of the initial condition.

Consider a biphoton wave traveling in the z direction. Because the sinc function factorizes in the transversal (x, y) directions for typical experimental parameters, we may disregard the x direction. In the case of a multislit diffraction, we could consider such waves impinging on a screen with slits along the x axis and study the spreading along the y axis. Thus assuming symmetry along the x axis, we may disregard the x coordinate. Now, for the sake of clarity, we follow [33] and consider a monochromatic wave function traveling in the positive z direction,

$$\Psi(y, z, t) = \psi(y, z) e^{-i\omega_0 t}, \tag{47}$$

in which ψ satisfies the Helmholtz equation $\triangle\psi = -k_0^2\psi$ and

$$\omega_0 = \begin{cases} ck_0, & \text{e.m. waves,} \\ \frac{\hbar k_0^2}{2m} & \text{de Broglie waves.} \end{cases}$$

Performing the one-dimensional Fourier transform,

$$\psi(y, z) = \frac{1}{\sqrt{2\pi}} \int \tilde{\psi}(k_y, z) e^{ik_y y} \, dk_y, \tag{48}$$

and using that $\psi(y, z)$ satisfies the Helmholtz equation yields, for progressive waves in the z direction,

$$\tilde{\psi}(k_y, z) = \tilde{\psi}(k_y, 0) e^{i\sqrt{k_0^2 - k_y^2} z}. \tag{49}$$

Therefore,

$$\psi(y, z) = \frac{1}{\sqrt{2\pi}} \int \tilde{\psi}(k_y, 0) e^{i(\sqrt{k_0^2 - k_y^2} z + k_y y)} \, dk_y, \tag{50}$$

which, in the Fresnel approximation $\sqrt{k_0^2 - k_y^2} \approx k_0 - k_y^2/(2k_0)$, yields [33]

$$\psi(y, z) = e^{ik_0 z} \frac{k_0}{\sqrt{2\pi i z}} \int e^{i\frac{k_0}{2z}(y - y')^2} \psi(y', 0) dy'. \tag{51}$$

Identifying $\psi(y, t = 0) \equiv \psi(y, z = 0)$ leads to $|\psi(y, t)|^2 \equiv |\psi(y, z)|^2$ provided $z = t/c$. This is based on the analogy between the paraxial Helmholtz equation and the Schrödinger equation for a free particle in two transverse dimensions:

$$\frac{\partial^2 A}{\partial x^2} + \frac{\partial^2 A}{\partial y^2} = ik_0 \frac{\partial A}{\partial z} \sim \frac{\partial^2 \Psi}{\partial x^2} + \frac{\partial^2 \Psi}{\partial y^2} = i\frac{2m}{\hbar} \frac{\partial \Psi}{\partial z}, \tag{52}$$

which allows us to relate the time evolution to the field's propagation [11]; in Eq. (52), $A = A(x, y, z)$ corresponds to, for example, a wave's amplitude and k_0 is characteristic of the pump. That said, we are led to a nonrelativisticlike propagator:

$$G(y, t; y', t') = e^{-i\frac{\tilde{m}c^2}{\hbar}(t - t')} \sqrt{\frac{\tilde{m}}{2\pi i\hbar(t - t')}} e^{i\frac{\tilde{m}(y - y')^2}{2\hbar(t - t')}}, \tag{53}$$

where

$$\tilde{m} \equiv \frac{k_0 \hbar}{c}. \tag{54}$$

The propagator (53) was used in [21] in a double slit experiment to demonstrate that a degenerate biphoton of wavelength λ produced via SPDC can behave as a single quantum of wavelength $\frac{\lambda}{2}$ as seen in [16]. Thus, we write the free propagation of a biphoton SPDC wave function as

$$\Psi(y_i, y_s, t) = \iint dy_i' \, dy_s' \; G(y_i, t; y_i', 0) G(y_s, t; y_s', 0) \times \Psi(y_i', y_s', 0). \tag{55}$$

The Wigner function propagator can be defined as [34]

$$W(y_i, q_i; t_i) = \iint dy_i^0 \, dq_i^0 \; K\big(y_i, q_i, t_i; y_i^0, q_i^0, 0\big) \times W\big(y_i^0, q_i^0; 0\big), \tag{56}$$

where

$$K\big(y_i, q_i, t_i; y_i^0, q_i^0, 0\big) = \frac{1}{2\pi} \iint dz_i \, dz_i^0 \; e^{i(z_i^0 q_i^0 - z_i q_i)} \times G^*\left(y_i - \frac{z_i}{2}, t; y_i^0 - \frac{z_i^0}{2}, 0\right) \times G\left(y_i + \frac{z_i}{2}, t; y_i^0 + \frac{z_i^0}{2}, 0\right), \tag{57}$$

which, for a free evolution, simplifies to

$$K_0\big(y_i, q_i, t_i; y_i^0, q_i^0, 0\big) = \delta\left(y_i - y_i^0 - \frac{q_i}{k_0} c\, t\right) \delta\big(q_i - q_i^0\big) \equiv \frac{c}{k_0} \delta\big(y_i - y_i^0 - v_i t\big) \delta\big(v_i - v_i^0\big)$$

with $v_i \equiv (cq_i)/k_0$. Hence

$$W(y_i, y_s, q_i, q_s, t_i, t_s) = W(y_i - v_i t_i, y_s - v_s t_s, q_i, q_s, 0, 0), \tag{58}$$

which in the variables expressed by Eq. (38) reads

$$W(y_+, y_-, q_+, q_-, \tau_1, \tau_2) = W_S(y_- - (v_-\tau_1 + v_+\tau_2), q_-) \times W_G(y_+ - (v_-\tau_2 + v_+\tau_1), q_+), \tag{59}$$

where $\tau_1 = (t_i + t_s)/2$ and $\tau_2 = (t_i - t_s)/2$ and $v_\pm \equiv (cq_\pm)/k_0$. Finally, the biphoton two-time transversal position

amplitude is obtained by integrating over momenta:

$$\mathcal{W}(y_+, y_-, \tau_1, \tau_2) = \iint dq_-\, dq_+\, W(y_+, y_-, q_+, q_-, \tau_1, \tau_2). \tag{60}$$

Following [4,5] we can write a continuous-variable Bell inequality with sign binning by defining the probability that measurements of q_i and q_s disagree in sign, namely, $P(+-) \cup P(-+)$. This is obtained by evaluating

$$\mathcal{D}(t_i, t_s) = \int_0^\infty dy_i \int_{-\infty}^0 dy_s\, \mathcal{W}(y_i, y_s, t_i, t_s) + \int_{-\infty}^0 dy_i \int_0^\infty dy_s\, \mathcal{W}(y_i, y_s, t_i, t_s), \tag{61}$$

which in $y_\pm$ variables reads

$$\mathcal{D}(t_i, t_s) = \int_0^\infty dy_- \int_{-y_-}^{y_-} dy_+\, \mathcal{W}(y_+, y_-, \tau_1, \tau_2) + \int_{-\infty}^0 dy_- \int_{y_-}^{-y_-} dy_+\, \mathcal{W}(y_+, y_-, \tau_1, \tau_2). \tag{62}$$

Following [4], consider the CHSH Bell inequality:

$$\mathcal{E}(t_i, t_s) + \mathcal{E}(t_i, t_s') + \mathcal{E}(t_i', t_s) - \mathcal{E}(t_i', t_s') \leqslant 2\,, \tag{63}$$

where

$$\begin{aligned}\mathcal{E}(t_i, t_s) &= P(++) + P(--) - P(+-) - P(-+) \\ &= 1 - 2[P(+-) + P(-+)] \\ &= 1 - 2\,\mathcal{D}(t_i, t_s).\end{aligned} \tag{64}$$

Hence (63) becomes

$$\mathcal{D}(t_i, t_s) + \mathcal{D}(t_i, t_s') + \mathcal{D}(t_i', t_s) - \mathcal{D}(t_i', t_s') \geqslant 0. \tag{65}$$

Equations (60) to (62) can be integrated using that

$$\int_{-\infty}^{+\infty} e^{ax^2+bx}\, dx = \sqrt{\frac{\pi}{-a}}\, e^{-\frac{b^2}{4a}}, \tag{66}$$

if $\mathrm{Re}(a) < 0$ and divergent otherwise, with $a, b \in \mathbb{C}$.

IV. RESULTS

The study of the Bell-like inequality (65) for a biphoton wave function is possible beyond double-Gaussian approximation. The problem becomes analytically tractable due to the expansion represented by Eq. (44) which can be integrated as shown in the Appendix. The summations can be easily performed using MATHEMATICA. In order to further simplify the analysis, we shall assume that the idler and signal photons emerge with momentum components such that $q_i + q_s = 0$. We further assume that we may neglect the Gaussian part of the total Wigner function (38), which makes sense in the limit $\sigma_+^2 \gg \sigma_-^2$ (experimentally one has typical values of $\sigma_+ = 1$ mm and $\sigma_- = 0.01$ mm [5] but we chose $\sigma_+^2 = 8$ and $\sigma_-^2 = 1/4$). Such hypotheses greatly simplify the expression for $\mathcal{D}(t_i, t_s)$ in (62), which becomes a function of $\tau_1 \equiv (t_i + t_s)/2$ only. Numerically it turns out that taking $M = 6$ is good enough to establish convergence. Thus $\mathcal{D}(t_i, t_s) = \mathcal{D}(\tau_1)$. Just as in [4] we may choose

$$t_i' = 0, \quad t_s = \tau_1, \quad t_i = -2\tau_1, \quad t_s' = 3\tau_1 \tag{67}$$

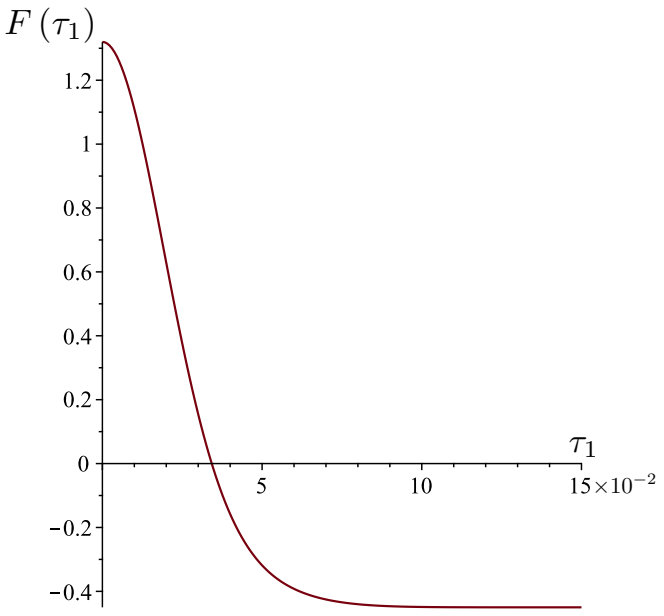

FIG. 5. $F(\tau_1)$ vs τ_1. We notice a violation of Eq. (68) for τ_1 just over 3×10^{-2}. Because τ_1 is the average of the signal's and idler's propagation times (t_s and t_i, respectively), this means the violation happens only after a certain time, $\tau_1 \gtrsim 3 \times 10^{-2}$, and stabilizes after it.

in (65). In addition, we also have $\mathcal{D}(t_i, t_s) = f(|\tau_1|)$. Hence we are led to express Eq. (65) as

$$F(\tau_1) \equiv 3f(\tau_1) - f(3\tau_1) \geqslant 0, \tag{68}$$

the graph of which is depicted in Fig. 5.

V. CONCLUSIONS

Bell nonlocality in continuous variables is hard to verify because continuous-variable quantum states usually have positive-definite Wigner functions that give support to local hidden variable models. In [5] Bell's approach was adapted to photon pairs. The authors of that study showed that the transverse positions and momenta of entangled photon pairs measured at different propagation distances can be used to find a maximum achievable violation for the state that Bell considers. It turns out it is very small relative to the upper limit of $2\sqrt{2}$.

In this paper, we aimed at qualitatively analyzing the possibility of continuous-variable Bell violation using a physical description in terms of biphoton wave functions. After carefully exposing the approximations that led to the effective biphoton wave function (produced by SPDC type-I processes) as well as its time evolution, we proposed a way of analytically treating the sinc function which represents the transverse propagation of the biphoton. We concluded that this more physical realization of the biphoton wave function leaves room for a continuous-variable Bell inequality violation as one can see in Fig. 5. A more realistic quantitative prediction of the violation can in principle be inferred using experimental input of SPDC processes and some numerical computation. Of course the parameters should be adjusted so as to guarantee local causality (that is to say, a spacelike separation for

the spacetime coordinates of the biphotons $|y_-| > c|\tau_2|$ as discussed in [4]).

As we have shown in Sec. II B, a high degree of entanglement is maintained in the limit where σ_- is small (as compared with σ_+), which is the approximation we have used to study the violation of positiveness of the function $F(\tau_1)$. We will address this matter in a future contribution.

ACKNOWLEDGMENTS

J.B.A. is thankful to Conselho Nacional de Desenvolvimento Científico e Tecnológico (CNPq) for the Grant No. 150190/2019-0. I.G.P. thanks CNPq. H.A.S.C. and C.H.S.V. are grateful to Coordenação de Aperfeiçoamento de Pessoal de Nível Superior (CAPES). M.S. thanks CNPq for the Grant No. 303482/2017, and Fundacão de Amparo à Pesquisa do Estado de São Paulo (FAPESP) for the Grant No. 2018/05948-6.

APPENDIX

Consider the integral

$$\mathcal{I} = \int d\rho\, e^{-2i\rho y} \cos[m'(q-\rho)^2] \cos[n'(q+\rho)^2] \tag{A1}$$

with $m' = \frac{2m-1}{2^M}$ and $n' = \frac{2n-1}{2^M}$. Assume $m' \neq n'$(that is $m \neq n$) and $m', n' > 0$. Thus,

$$\mathcal{I} = \int d\rho\, e^{-2i\rho y} \frac{e^{im'(q-\rho)^2} + e^{-im'(q-\rho)^2}}{2} \times \frac{e^{in'(q+\rho)^2} + e^{-in'(q+\rho)^2}}{2}, \tag{A2}$$

which in turn may be cast as

$$\mathcal{I}_{m' \neq n'} = \tfrac{1}{4}(\mathcal{I}_1 + \mathcal{I}_2 + \mathcal{I}_3 + \mathcal{I}_4), \tag{A3}$$

with

$$\mathcal{I}_1 = \int d\rho\, e^{i\,[m'(q-\rho)^2 + n'(q+\rho)^2 - 2\rho y]}, \tag{A4}$$

$\mathcal{I}_2 = \mathcal{I}_1(n' \to -n')$, $\mathcal{I}_3 = \mathcal{I}_1(m' \to -m')$, and $\mathcal{I}_4 = \mathcal{I}_1(n' \to -n'$ and $m' \to -m')$. Completing squares we get

$$\mathcal{I}_1 = e^{-i\frac{(m'q-n'q+y)^2}{(m'+n')} + i\,(m'+n')q^2} \times \int d\rho\, e^{i\,(\sqrt{m'+n'}\rho - \frac{(m'q-n'q+y)}{\sqrt{m'+n'}})^2}. \tag{A5}$$

This evaluates to

$$\mathcal{I}_1 = e^{-i\frac{(m'q-n'q+y)^2}{(m'+n')} + i\,(m'+n')q^2} \frac{\sqrt{\frac{\pi}{2}}(1+i)}{\sqrt{m'+n'}}.$$

Likewise

$$\mathcal{I}_2 = e^{-i\frac{(m'q+n'q+y)^2}{(m'-n')} + i\,(m'-n')q^2} \begin{cases} \frac{\sqrt{\frac{\pi}{2}}(1+i)}{\sqrt{m'-n'}}, & m' > n' \\ \frac{\sqrt{\frac{\pi}{2}}(1-i)}{\sqrt{n'-m'}}, & m' < n', \end{cases}$$

$$\mathcal{I}_3 = e^{-i\frac{(-m'q-n'q+y)^2}{(-m'+n')} + i\,(-m'+n')q^2} \begin{cases} \frac{\sqrt{\frac{\pi}{2}}(1-i)}{\sqrt{m'-n'}}, & m' > n' \\ \frac{\sqrt{\frac{\pi}{2}}(1+i)}{\sqrt{n'-m'}}, & m' < n', \end{cases}$$

and

$$\mathcal{I}_4 = e^{-i\frac{(-m'q+n'q+y)^2}{(-m'-n')} + i\,(-m'-n')q^2} \frac{\sqrt{\frac{\pi}{2}}(1-i)}{\sqrt{m'+n'}}$$

for $m' \neq n'$. On the other hand, for $m' = n'$,

$$\mathcal{I}_{m'=n'} = \frac{2}{4}\,\mathrm{Re}\left[e^{-i\frac{y^2}{2m'} + 2im'q^2} \frac{\sqrt{\frac{\pi}{2}}(1+i)}{\sqrt{2m'}}\right]. \tag{A6}$$

For this result we have chosen $\sigma_-^2 = 1/4$ but for arbitrary σ_- it suffices to multiply the overall result by $(2\sigma_-)^{-1}$ and rescale $y \to \frac{y}{2\sigma_-}$ and $q \to 2\sigma_- q$.

[1] A. Acín, N. Brunner, N. Gisin, S. Massar, S. Pironio, and V. Scarani, Phys. Rev. Lett. **98**, 230501 (2007).
[2] A. F. Abouraddy, T. Yarnall, B. E. A. Saleh, and M. C. Teich, Phys. Rev. A **75**, 052114 (2007).
[3] W. J. Munro, Phys. Rev. A **59**, 4197 (1999); J. Wenger, M. Hafezi, F. Grosshans, R. Tualle-Brouri, and P. Grangier, *ibid.* **67**, 012105 (2003); H. Nha and H. J. Carmichael, Phys. Rev. Lett. **93**, 020401 (2004); R. García-Patrón, J. Fiurášek, N. J. Cerf, J. Wenger, R. Tualle-Brouri, and P. Grangier, *ibid.* **93**, 130409 (2004); R. García-Patrón, J. Fiurášek, and N. J. Cerf, Phys. Rev. A **71**, 022105 (2005); A. Acín, N. J. Cerf, A. Ferraro, and J. Niset, *ibid.* **79**, 012112 (2009).
[4] J. S. Bell, *Speakable and Unspeakable in Quantum Mechanics*, 1st ed. (Cambridge University, New York, 1987); Ann. N.Y. Acad. Sci. **480**, 263 (1986).
[5] J. Schneeloch, Samuel H. Knarr, D. J. Lum, and J. C. Howell, Phys. Rev. A **93**, 012105 (2016).
[6] J. F. Clauser, M. A. Horne, A. Shimony, and R. A. Holt, Phys. Rev. Lett. **23**, 880 (1969).
[7] Y. Shih, *An Introduction to Quantum Optics: Photon and Biphoton Physics*, Series in Optics and Optoelectronics (Taylor & Francis, London, 2014).
[8] G. Milione, S. Evans, D. A. Nolan, and R. R. Alfano, Phys. Rev. Lett. **108**, 190401 (2012); F. Cardano, E. Karimi, S. Slussarenko, L. Marrucci, C. de Lisio, and E. Santamato, Appl. Opt. **51**, C1 (2012); A. Vaziri, G. Weihs, and A. Zeilinger, Phys. Rev. Lett. **89**, 240401 (2002).
[9] D. C. Burnham and D. L. Weinberg, Phys. Rev. Lett. **25**, 84 (1970).
[10] A. S. Friedman, A. H. Guth, M. J. W. Hall, D. I. Kaiser, and J. Gallicchio, Phys. Rev. A **99**, 012121 (2019).
[11] J. Schneeloch and J. C. Howell, J. Opt. **18**, 053501 (2016).
[12] S. P. Walborn, C. H. Monken, S. Pádua, and P. H. Souto Ribeiro, Phys. Rep. **495**, 87 (2010).
[13] C. Couteau, Contemp. Phys. **59:3**, 291 (2018).
[14] L. Mandel and E. Wolf, *Optical Coherence and Quantum Optics* (Cambridge University, Cambridge, England, 1995).

[15] R. Menzel, *Photonics* (Springer-Verlag, Berlin, 2007).
[16] E. J. S. Fonseca, C. H. Monken, and S. Pádua, Phys. Rev. Lett. **82**, 2868 (1999); C. H. Monken, P. H. S. Ribeiro, and S. Pádua, Phys. Rev. A **57**, 3123 (1998).
[17] D.-J. Zhang, S. Wu, H.-G. Li, H.-B. Wang, J. Xiong and K. Wang, Sci. Rep. **7**, 17372 (2017).
[18] E. T. Jaynes and F. W. Cummings, Proc. IEEE **51**, 89 (1963); F. W. Cummings, Phys. Rev. **140**, A1051 (1965).
[19] C. K. Law and J. H. Eberly, Phys. Rev. Lett. **92**, 127903 (2004).
[20] M. V. Fedorov, Y. M. Mikhailova, and P. A. Volkov, J. Phys. B **42**, 175503 (2009).
[21] A. Paul and T. Qureshi, Quanta **7**, 1 (2018).
[22] A. Bramon and R. Escribano, arXiv:quant-ph/0507040v2.
[23] J. C. Howell, R. S. Bennink, S. J. Bentley, and R. W. Boyd, Phys. Rev. Lett. **92**, 210403 (2004); M. Edgar, D. Tasca, F. Izdebki, R. Warburton, J. Leach, M. Agnew, G. Buller, R. Boyd, and M. Padgett, Nat. Commun. **3**, 1 (2012); R. S. Bennink, S. J. Bentley, R. W. Boyd, and J. C. Howell, Phys. Rev. Lett. **92**, 033601 (2004); I. A. Khan and J. C. Howell, Phys. Rev. A **73**, 031801(R) (2006).
[24] M. R. A. Adcock, P. Hoyer and B. C. Sanders, Quant. Info. Proc. **12**, 1759 (2013).
[25] S. M. Abrarov and B. M. Quine, Appl. Numer. Math. **150**, 65 (2020); B. M. Quine and S. M. Abrarov, J. Quant. Spectrosc. Radiat. Transfer **127**, 37 (2013).
[26] I. Bialynicki-Birula, J. Opt. **19**, 12 (2017).
[27] O. Keller, *Light: The Physics of the Photon*, Series in Optics and Optoelectronics (CRC, Boca Raton, FL, 2014).
[28] B. J. Smith and M. G. Raymer, New J. Phys. **9**, 414 (2007).
[29] J. H. Field, Ann. Phys. (NY) **321**, 627 (2006).
[30] O. Keller, Phys. Rev. A **62**, 022111 (2000)
[31] P. L. Saldanha and C. H. Monken, New J. Phys. **13**, 073015 (2011).
[32] I. Bialynicki-Birula, Acta Phys. Pol. A **86**, 97 (1994); *Photon Wave Function*, edited by E. Wolf, Progress in Optics Vol. 36 (Elsevier, Amsterdam, 1996); J. E. Sipe, Phys. Rev. A **52**, 1875 (1995).
[33] G. Dillon, Eur. Phys. J. Plus **127**, 66 (2012).
[34] T. Takabayasi, Prog. Theor. Phys. **11**, 341 (1954).